Body and Surface Wave Ambient Noise Seismic Interferometry Across the Salton Sea Geothermal Field, California

Lindsay Erin Sabey

Thesis submitted to the faculty of the Virginia Polytechnic Institute and State University in partial fulfillment of the requirements for the degree of

Master of Science

In

Geosciences

John A. Hole

Martin C. Chapman

Ying Zhou

November 10, 2014

Blacksburg, Virginia

Keywords: Ambient noise, passive source imaging, seismic interferometry, multimodal surface waves, reflection imaging

Body and Surface Wave Ambient Noise Seismic Interferometry Across the Salton Sea Geothermal Field, California

Lindsay Sabey

ABSTRACT

Virtual source gathers were generated using the principles of seismic interferometry from 135 hours of ambient noise recorded during a controlled-source survey across the Salton Sea Geothermal Field in southern California. The non-uniform nature of the noise sources violated a primary assumption of the method and generated artifacts in the data. The artifacts generated by the high-energy impulsive sources (e.g. earthquakes, shots) were removable using traditional methods of amplitude normalization prior to cross-correlation. The continuous source artifacts generated by the geothermal wells and highways required an unconventional approach of utilizing only normalized impulsive sources to successfully reduce the artifacts. Virtual source gathers were produced successfully that contained strong surface waves at 0.4-2.5 Hz, an order of magnitude below the corner frequency of the geophones, and modest body waves at 22-30 Hz, which are generally more difficult to obtain due to the need for many large, well-distributed subsurface sources. The virtual source gathers compare well to nearby explosive shots and are more densely spaced, but have a much lower signal-to-noise ratio. Analysis of the surface waves was complicated by strong higher-order modes. Spectral analysis of virtual source gathers required utilization of the geothermal plant energy, which produced usable signal at offsets required for mode separation. The virtual source dispersion curve compared well to a dispersion curve from a nearby explosive shot. P-waves were observed on the virtual source gathers. Creation of a low-quality multichannel reflection stack revealed two weak reflectors in the upper 2 km.

ACKNOWLEDGEMENTS

I would like to offer my gratitude to my advisor and committee for all their wisdom and guidance to bring this manuscript to fruition. A special thank you to my advisor for this opportunity to journey through graduate school and work on this project.

The Salton Seismic Imaging Project was funded by National Science Foundation grants OCE-0742263 to Virginia Tech and OCE-0742253 to Caltech, and by the United States Geological Survey's Multi-Hazards Program. Numerous landowners, native American tribes, and government agencies provided permission to work on their land. IRIS-PASSCAL provided the seismic instruments and field support. Over 100 volunteers, mostly students, assisted with the fieldwork. The seismic data are archived at the IRIS Data Management Center.

DEDICATION

To my family for all their wonderful love and support that kept me strong whenever there was doubt. To my friends for all the laughter and fun times that made graduate school so enjoyable. Finally and most importantly, to my two beautiful children that have motivated and inspired me to achieve all our dreams and I hope one day you will strive for the same. I am so grateful for all of you, without your continuous love and support none of this would have been possible.

TABLE OF CONTENTS

LIST OF FIGURES

LIST OF TABLES

INTRODUCTION

Seismic interferometry allows the creation of "virtual sources" from ambient-noise, turning traditionally nuisance noise into useful signal. The method involves cross-correlation of noise from pairs of seismometers to extract Earth's Green's Function for a source at the reference seismometer. In a 1-dimensional medium, a plane wave reflection response of a surface source can be obtained through autocorrelation of the transmission response (Claerbout, 1968). This is transferable to a 3-dimensional medium by utilizing the reciprocity theorem and conservation of energy (Wapenaar et al., 2002). Applicable to any lossless, heterogeneous medium, cross-correlation of two seismic traces recorded at separate receiver locations yields the impulse response at one location as if there was a source at the other (Wapenaar, 2002).

Seismic interferometry has found useful application across a broad range of communities. Interest in surface waves has emerged in the last decade (Campillo and Paul, 2003; Sabra et al., 2005; Shapiro et al., 2005), resulting in numerous studies that have used long-period energy to image the crust and lithosphere (Lin et al., 2008; Yang et al., 2010; Saygin and Kennett, 2012). Surface-wave noise at much higher frequency is used for geotechnical applications at tens of meters depth (Louie, 2001). More recently, surface wave noise recorded during an industry survey provided information about the upper ~800 m, which aided processing of the multichannel reflection data (Lin et al., 2013). Surface wave coda of earthquake sources has also found use in seismic interferometry to monitor changes over time for earthquake hazard and volcano studies (Sneider, 2004; Wegler et al., 2007; Haney et al., 2009).

Extraction of body-waves has been more challenging because most natural noise is surface waves. However, there have been a few successes in retrieving direct and reflected waves (Sneider, 2004; Roux et al, 2005; Dragonov et al., 2007; Schuster, 2010; Byerly et al., 2010; Ryberg, 2011; Lin and Tsai, 2013). Subsurface sources are required to produce body waves, making the coda of earthquakes or controlled sources more useful than long-duration ambient noise. For both body and surface waves, the recent development in industry of continuously recorded, non-cabled systems provides a potential opportunity to utilize ambient-noise interferometry on large, densely sampled arrays. (Figure 1). Due to abundant local micro-seismicity and active geothermal energy production, this line was a seemingly ideal prospect for ambient noise seismic interferometry. This thesis/manuscript describes the application of interferometry methods to SSIP data to derive virtual source gathers that constrain shallow structure across the geothermal field.

TECTONIC AND GEOLOGIC SETTING

The Salton Trough is part of the active Gulf of California rift system that is moving the Baja California peninsula away from Mexico (Figure 1). The Salton rift basin links the southernmost terminus of the transform San Andreas Fault to the transform Imperial Fault (Figure 2). The Salton Trough was once connected to the Gulf of California and has undergone rapid extension and infill of sediment from the Colorado River. Sediment build-up has isolated the present day Salton Trough from the Gulf of California, but remains below sea level.

The transtensional shear zone between the San Andreas Fault and the Imperial fault is expressed through an oblique zone of faulting that form the present day Brawley

Seismic Zone (Figure 2; Fuis and Kohler, 1984). Previous studies have identified abandoned fault segments such as the Brawley, Calipatria, and Wister Faults (Meidav and Fergerson, 1972; Chan and Tewhey, 1977; Lynch and Hudnut, 2008). Mapped faults within the Brawley Seismic Zone are very steeply dipping and have a combination of normal and strike-slip motion (Sylvester and Smith, 1976; Rogers, 1980; Brothers et al., 2011). The extending basin of the Salton Trough was filled with marine sediments of the Imperial Formation during the Pliocene while it was connected to the Gulf of California (Figure 3a). Eventually the Colorado River delta built up enough sediment within the Palm Springs Formation (Figure 3a) to isolate the northern portion of the Salton Trough from the Gulf of California. Re-direction of the Colorado River led to the formation of ancient freshwater Lake Cahuilla in the depression north of the delta (Figure 2). The lake periodically filled up and evaporated in response to the course of the Colorado River, leading to a transition from marine-deltaic deposits to the alternating contribution of lacustrine and evaporitic sediments of the Borrego and Brawley Formations with interfingering alluvial flanks from the Ocotillo Formation (Figure 3; Van de Kamp, 1973; Younker et al., 1981; Lonsdale, 1989; Dorsey, 2010). A regional unconformity is noted between the fine-grained sediments of the perennial lakebeds that make up the Borrego Formation and the sandier playa-like lacustrine-deltaic deposits of the Brawley Formation (Dibblee, 1954; Dutcher et al., 1972; Lutz et al., 2006; Kirby et al., 2007; Janecke et al., 2010).

Within the valley, the Salton Sea Geothermal Field covers about half of the Imperial Valley seismic line. It is one of the largest and hottest geothermal fields in North America with temperatures reaching up to 300˚C at 1km depth and spanning approximately 26 km^2 (Elders, 1989; Svenson et al. 2007). Shallow magmatism

associated with rifting, accompanied by several rhyolitic intrusions, provides a prolific heat source to the system (Kasameyer et al, 1984; Hulen and Pulka, 2001; Hulen et al., 2002; Schmitt, 2008).

A series of wells were drilled and tested during the 1960s and 1970s as a part of the Salton Sea Scientific Drilling Project (Muramoto and Elders, 1984). The stratigraphy of the field can be broken down into four sections: a shallow basement, a lower hydrothermally altered reservoir, an upper unaltered reservoir, and a shallow low permeability cap overlain by unconsolidated sediment (Figure 3; Towse and Palmer, 1975; Morse, 1977; Younker et al., 1981). The crystalline basement occurs as shallow at 2km depth within the geothermal field and consists of late-Pliocene sediment metamorphosed by the high heat flow (Figure 3; Schroeder, 1976). Directly above the basement is the lower portion of the reservoir that is composed of the fluvial-deltaic sediments of the Palm Springs Formation that have undergone hydrothermal metamorphism from the high temperatures and hypersaline brines. Epidote and silica cementation has greatly reduced the permeability and porosity in the lower reservoir leading to the velocity increase reported on sonic logs (Figure 3, Younker, 1978; Sturz, 1989). Fluid circulation within the lower reservoir is reliant on secondary porosity and permeability from natural and induced fractures (Tewhey, 1977; Dept. of Energy, 2004; Norton and Hulen, 2006). Networks of steeply dipping transtensional faults are seen in both the onshore and offshore portions of the geothermal field (Hulen et al., 2003a; Brothers et al., 2011; Bianco, 2012). The degree of alteration and a thin shale layer separate the reservoir into an upper and lower portion (Schroeder, 1976; Morse, 1977; McDowell and Elders, 1983). The reservoir contains sediments from the lower Borrego Formation and is approximately 600-m thick (Herzig et al., 1988). It was the most easily

correlated sequence of strata from well logs since the degree hydrothermal alteration increases rapidly with depth. The impermeable shales and interbedded anhydrite-rich evaporate layers of the upper Borrego Formation contain the reservoir (Tewhey, 1977). The geothermal system is self-healing and at the same time continuously being faulted. As fractures are continuously broken, the hydrothermal system reseals through circulation of heated fluids that cause thermal alteration and mineral deposition along flow paths (Batzle and Simmons, 1976; Younker et al., 1981; McKibben and Andes, 1986). The entire sequence thickens northward and to a lesser degree eastward as it marks the period of continuous refilling and draining of the Salton Sea after the separation from the Gulf of California (Chan and Tewhey, 1977; Morse, 1977; Younker and Kasameyer, 1978; Dorsey, 2010).

SEISMIC DATA AND AMBIENT NOISE

The National Science Foundation and the United States Geological Survey funded the Salton Seismic Imaging Project to acquire seismic reflection and refraction data with the goals of understand faulting and rift processes and earthquake hazard within the basin (Han et al., 2013). Data were acquired in March 2011, including a seismic line of 486 seismometers deployed across the Imperial Valley, the Brawley Seismic Zone, and the Salton Sea Geothermal Field. The 4.5-Hz seismometers and REFTEK “Texan” seismographs were deployed along a crooked line at 500m spacing in the western mesa, 100m spacing in the valley floor, and 300m spacing in the eastern mesa (Figure 2). The seismographs were deployed twice, and each time were set to record continuously for as long as the internal power (two C cells) could last. In addition to eighteen explosive shots on line and many off line, 135 hours of ambient noise were recorded.

Understanding the noise sources is important for the generation of virtual source gathers. Noise sources can be characterized by their location and primary energy contribution (body wave vs. surface wave), frequency content, distribution, and duration. The identified noise sources within this dataset included: geothermal plant and well pumping operations, induced and natural seismicity, two highways and a railroad that cross the line, explosive shots from the survey, military operations, waves from the Salton Sea, and agricultural operations (Figure 4). Over 300 local microearthquakes with magnitudes < 2 were identified in the 135-hour dataset. During the same times, the Southern California Seismic Network recorded only three events of magnitudes 0.5-1.6. All on-line and many off-line explosive shots were clearly visible in the data (Figure 9). In the valley, explosive shots were drilled to depths of ~25m in water saturated sediments and loaded with 115-229kg of explosives. In the alluvial mesas that flank the valley, the shot holes were drilled to a depth of 25-32m and loaded with 230-480kg of explosives. Seven actively producing geothermal plants are along the line, but the Vulcan Geothermal Power Plant produced by far the most noise (Figure 7). The explosive shots, earthquakes, and underground geothermal facilities likely provided the primary subsurface body-wave noise sources. While the many active faults in the region allowed for a broad distribution of earthquakes, the geothermal wells were contained to the geothermal field in the eastern half of the valley. The other identified noise sources contribute primarily surface waves.

The noise sources can also be categorized based on duration as impulsive point and continuous sources. Impulsive point sources are short duration, high-energy sources such as explosive shots and earthquakes. Continuous sources are low-energy sources that last indefinitely or for an extended period of time. The geothermal pumping wells

acted as continuous, stationary sources that remained constant throughout the survey. The highways and railroad acted as repeated sources, and since they were oriented roughly perpendicular to the seismic line they acted as relatively localized sources. Military sources included bombing and artillery ranges on the mesas on both ends of the line and associated jets. Highways, railroad, and military noise contained mostly higher frequencies >1Hz, geothermal operations were strong at lower frequencies <1Hz, and earthquakes overlapped both frequency ranges (Figure 4).

GENERATING VIRTUAL SOURCE GATHERS

Prior to processing, the 135 hours of continuously recorded data were cut into 2-minute windows and quality control was performed on the raw data revealing over 300 earthquakes (M<2) in the dataset. The two-minute windows containing earthquakes and known active shots were separated from the raw noise data.

Ambient noise data were processed following a method similar to Bensen et al. (2007) to create virtual source gathers (Table 1). Data underwent spectral whitening to broaden the bandwidth of recorded noise between 0.1 and 50Hz. Amplitude normalization was applied in the form of an automatic gain control (AGC) filter. Both the spectral whitening and AGC were necessary to attenuate dominant noise sources, such as the earthquakes, shots, and geothermal power plants. A pilot trace from a given reference receiver was cross-correlated against all other traces and stacked to produce a “virtual source” gather for that receiver location (Figure 5). This was repeated for all receiver stations to yield a total of 486 virtual source gathers. Both surface and P-waves in the virtual source gathers have apparent velocities comparable to those observed in nearby explosive shot gathers (Figures 9, 13). The virtual source gathers contain much

lower energy and lower frequency, but provide 486 virtual sources to supplement the sparser and more expensive explosions. The virtual shots have a zero-phase wavelet (traces are a band-limited Green's function), while the explosions produce a causal wavelet.

The ambient noise data were cross-correlated for positive and negative time so that a successful gather should take the shape of an "X" for both body and surface waves (Figure 5). Since most ambient noise is surface waves, they dominate the virtual source gathers below ~20 Hz and are the only "X" apparent on Figure 5. In order to see P-waves, a low-cut filter is required. Positive time represents energy that traveled from the virtual source to the receiver (shot gather) whereas negative time represents energy that traveled from the receiver to the virtual source (receiver gather). A lack of symmetry in amplitude and frequency content is apparent on Figure 5. The dominant left-going energy has lower frequency than the right-going energy. This is due to a violation of the assumption of a random, uniform source distribution.

Large impulsive events (such as earthquakes and explosive shots) can dominate the energy input into the virtual source gather and generate artifacts (Figure 6a). An artifact may be discernable if it travels only from the source to the receiver and not vice versa (Figure 7). The surface wave and body wave artifacts appear at different times and slopes (Figure 6a). The artifacts produced by large impulsive events are well understood, and prevented by attenuating or removing them from the dataset prior to cross-correlation (Bensen et al., 2007). With removal of only the nearby shots and largest earthquakes, nearly 10 hours of data containing impulsive events were retained without artifacts (Figure 6b). Inclusion of most of the impulsive sources works because their amplitudes were normalized, because there are a large number of them, and

because they are spatially distributed at a range of directions and distances surrounding the seismic line.

Unlike the impulsive sources, continuous point sources cannot be removed using traditional methods. Attenuation of amplitude is ineffective as the character of the wavelet stacks in over time to produce an artifact similar to what is generated by an impulsive source (Figure 7a). Stacking additional time only amplifies the artifact, as it is the most coherent noise at most times. The only mitigation is to reduce the time stacked into the virtual noise gathers, which contradicts the goal of accumulating sufficient random noise to find the interferometry signal.

Highway traffic artifacts were reduced by cross-correlating only nighttime hours when traffic was lower. The geothermal plant artifacts were more difficult to remedy. They appear similar to an impulsive source when the virtual source's reference station is close to the geothermal plant, but are observed as a point-source artifact at further distance (Figure 7). Reducing the artifact required an unconventional approach inspired by the assumptions of the method. Since the distribution of earthquake sources and far offset shots were successfully canceling with normalized amplitudes, cross-correlation was performed using only two-minute time windows containing the impulsive earthquake and explosion sources. The very largest earthquakes and closest shots were excluded. Approximately 6.5 hours of data were used, compared to the 135 hours of recorded data. This method allowed a sufficient amount of energy to be input into the system, with less time for the continuous source to be stacked. This use of impulsive sources rather than a long duration dominated by surface wave noise is also optimal for recovery of body waves (Lin and Tsai, 2013). The artifacts of the stationary continuous sources were

reduced except at closest proximity to the source and at the low frequencies in which the noise sources were dominant (Figure 8).

One of the goals was to produce body waves from the interferometry. Unfortunately, most previous work has demonstrated that the majority of the ambient noise is surface waves (Aki and Richards, 1980; Dong et al., 2006, Draganov et al., 2009; Forghani and Sneider, 2010; Ryberg, 2011), To overcome this, a sufficient amount of noise energy is required from subsurface sources (Campillo and Paul, 2003). The method described above to reduce the effects of continuous noise sources utilized the abundant local seismicity and explosions, potential sources of body waves. Virtual sources produced using only the impulsive sources produced visible P-waves (Figure 11).

The incorporation of different strategies based on noise characteristic allowed for significant reduction of artifact contamination and generation of successful virtual source gathers (Figures 5, 9, 11). Far from the roads and geothermal plants, the full 135 hours of ambient noise were cross-correlated. Near the roads, only nighttime data were used, when the roads were less active. Near the geothermal plants, only noise windows containing earthquakes and shots were used. In all cases, spectral whitening and AGC were required to balance the noise, and in no case were the very largest earthquakes or very closest explosive shots included.

SURFACE WAVES

Cross-correlation interferometry successfully produced surface waves throughout the seismic line (Figure 9b,c). The virtual sources recorded frequencies as low as 0.4Hz and up to 30 Hz. The explosive shots also produced useful surface-wave

energy down to 0.4 Hz (Figure 10). These observations are an order of magnitude below the 4.5 Hz corner frequency of the seismometer. The explosive shot gathers and higher quality virtual source gathers revealed the surface wave energy splitting into multiple packets with distinctly different velocities at far offset, interpreted to represent the fundamental and higher order modes (Figure 9). Higher-order modes have been observed in an earlier study south of our line but within the lacustrine sediments from ancient Lake Cahuilla (Barker and Stevens, 1983). Strong higher order modes may occur when there is a higher velocity layer over a lower velocity layer or in presence of a strong velocity increase with depth (Foti, 2000). Both cases are likely present in our area; the former is due to the impermeable lacustrine layer overlying an over-pressured zone. There are many artesian wells in the valley and overpressure was noted in many of the well log reports within the geothermal field (Figure 3, Holland, 2002;). In the geothermal field where the higher modes are most obvious, there is an added factor of fracturing within the geothermal field to contribute to the low-velocity zone (Setyowiyoto, 2012). With increasing depth, heat and fluid circulation cements the fractures and the velocity increases to 5km/s occurring at less than 2km depth in the geothermal field (Figure 3) and ~5km depth outside the geothermal field but within the valley.

Since the fundamental mode travelled at ~85-200m/s and the higher order modes travelled at 200-500m/s, the energy at far offsets from the source can be observed at two separate packages. This was easily observable on the explosive shot gathers that contained quality signal at >10km offset, however, the virtual source gathers only contained usable signal out to 4-7km leading to modal superposition in the near offsets (Figure 9). Further the virtual source gathers contained artifacts produced by the geothermal plant that dominated at low frequencies. At sufficient offset from the plant

(>2km), the cross-correlation of the source signal of the multiple modes produces four bands of energy (Figure 9b). When the virtual source station is in-line with the geothermal plant, the band of energy from the geothermal plant that goes through the location of the virtual source is usable signal representing the cross-correlation of the fundamental mode with the fundamental mode and the higher-order mode with the higher-order mode. The bands of energy above and below the desired surface wave packets represent the cross-correlation of the fundamental mode with the higher-order mode and drown out the desired signal of the virtual source surface waves propagating toward the geothermal plant.

Spectral analysis supports the interpretation of higher order modes, illustrated by multiple velocities at each frequency (Figure 10). The dispersion curves were computed for the surface waves using the method of velocity-spectral analysis (McMechan and Yedlin, 1981; Louie, 2001) (Table 2). Explosive shot gathers were windowed to an offset range with a good signal-to-noise ratio over a range of 5km where mode separation was apparent. Virtual shot gathers were limited by poorer signal quality and insufficient offset to observe mode separation at most locations. The highest signal quality on virtual sources was observed using the geothermal plant energy that crossed through the location of the virtual source. A 5-km distance range was used to minimize lateral changes in velocity (Figure 9B; Figure 10). A top mute was applied to remove body waves and high-order modes following suggestions from Ivanov et al. (2001). A bandpass filter of 0.1 to 3Hz removed unwanted high frequencies where the data was spatially aliased due to the 100-m station spacing and slow velocities of the unconsolidated sediments. Trace amplitudes were normalized by offset to account for spreading. A tau-p transform followed by a Fourier transform on tau was applied for the

velocities and frequencies of interest. Successful dispersion curves revealed bands of energy for the fundamental and higher-order modes (Figure 10). Windowing of the data to lower frequencies was necessary to see the attenuated energy at longer periods (Figure 10c). The peak energy for each mode was handpicked as a function of frequency to find the dispersive phase velocity curve. Overlapping modes on the virtual source gathers made only the highest quality gathers usable for dispersion analysis (Figure 10b). The dispersion curves for an explosive shot and nearby virtual source were compared with best agreement at lower frequencies between 1-1.5Hz (<5% error) and greater uncertainty at frequencies above 2Hz (10-13% error). This is expected for two reasons. First, the explosive shots had the advantage of signal quality at far offsets where the modes were distinctly separated, however, even the best quality virtual sources only contained surface wave signal out to ~7km so some of the higher modes were retained in the higher frequencies of the dispersion curve where the velocities were similar. Second, the higher frequencies attenuate faster so the virtual sources contained poorer signal quality at higher frequencies (Figure 10a). Inversion of the dispersion curves is possible to obtain the shallow shear velocity profile, though that is beyond the scope of this thesis. Recent studies have shown joint inversion of fundamental and higher-order modes to be possible and produce more detailed velocity analysis than with the fundamental mode alone (Park et al., 1999a; Park et al., 1999b, Park et al., 1999c; Xia et al., 2002; Xia et al., 2003). However, the inversion process becomes more complicated and careful precautions must be taken to avoid mode misidentification that can lead to large errors in the estimated shear wave velocity models (O'Neill, 2005; Boaga et al., 2013).

P-WAVES

P-waves are observed in the virtual source gathers only after application of a bandpass filter from 22 to 35Hz (Figure 11). Interferometry found the best P-waves in areas that had well-distributed subsurface noise sources, and at further distance from the strong surface-wave sources at the geothermal plants and highways. Direct and refracted P-waves were recorded at up to 4km offset, propagating at ~2 km/s in the unconsolidated sediment (Figure 11). A possible reflector was observed at between 0.7-1.2s throughout the valley and an additional reflector appeared around 2.4s in the geothermal field. Shallow reflectivity is difficult to observe in the explosive shot gathers, and shallow imaging is not possible due to the shot spacing of 1 to >5 km. While the signal-to-noise ratio is poor, the dense receiver spacing of the virtual sources effectively provides a “shot” every 100 meters and enables multichannel reflection imaging.

The virtual source gathers were processed and stacked using standard seismic reflection methods (Table 3), with the goal of illuminating the upper 2-3 km. The P-wave stacking velocity model was built from acoustic well logs in the geothermal field (Figure 3; Younker, 1981; Paillet et al., 1986; Daley et al. 1988, Bonner et al., 2006) and from first-arrival refraction tomography of the explosive shot data (Livers et al., 2012). The CMP spacing of 50-m resulted in a nominal 20-stack fold.

The stacked reflection section (Figure 12) is of poor quality due to the weak virtual-source signal, large station spacing (100 m), and low fold. Active-source reflection surveys have been acquired across the geothermal field for energy production, and imaging was complicated by abundant faulting and hydrothermal alteration (Helgeson, 1968; Browne, 1978; Gritto and Majer, 2003; Bianco, 2013). These sections are characterized by short (<2 km) reflection segments offset by faults, and a gradual loss of

coherent reflectivity below ~1 s. However, a possible weak band of reflectivity is observed across the entire valley at 0.8-1.2 s and a second, shorter band at ~2.3 s. An apparent offset in the reflectivity coincides with the steeply dipping Calipatria fault, one of a series of en echelon faults in the transition zone between the San Andreas and Imperial faults (Schroeder, 1976; Lynch and Hudnut, 2008; Tratt et al., 2009). The deeper reflectivity is present only in the geothermal field and is consistent with vertical seismic profile data obtained from State-well 2-14 (Figure 3; Daley, 1988; Bonner, 2006).

DISCUSSION

Seismic interferometry is an effective tool in a noisy environment with both surface and subsurface noise sources. However, the creation of virtual source gathers requires special attention to noise sources that violate the assumption of an even source distribution. Normalizing the amplitude prior to cross-correlation and deleting the largest events removed artifacts from large impulsive sources. For continuous or repeated sources, the noise persists throughout the data, so removal via traditional methods is not possible. Cross-correlating only the time windows that contain earthquakes and distant explosive shots, with amplitude normalization, contributed sufficient randomly distributed energy while reducing the artifact caused by the continuous source. One geothermal plant dominated at low frequencies despite such mitigation; however, when the stations are in-line with the geothermal plant and a sufficient distance away (>2km) the surface wave energy from the geothermal plant becomes desired usable signal.

Virtual source and explosive shot surface waves were observed at frequencies as low as 0.4Hz, despite being recorded on 4.5-Hz geophones. Shallow, unconsolidated sediment led to very slow surface wave velocities of 85-500m/s in the Imperial Valley.

The existence of strong higher order modes complicated the analyses because most of the virtual source gathers did not extend to sufficient offset to separate the modes in time. Surface wave energy from the geothermal plant produced usable signal at the farthest offsets. Artifacts produced from the cross-correlation of fundamental mode with higher-order modes, however, mask the desired signal of the virtual source surface waves propagating in the direction of the geothermal plant resulting in a predominately one-sided virtual source gather. The geothermal plant energy at an in-line virtual source produced a dispersion curve that was agreeable to a dispersion curve from a nearby explosive shot. The dispersion curve picks compared best at lower frequencies where the signal was most dominant in the virtual source gathers. Due to the weaker signal, geothermal plant artifacts, and overlapping modes, only a handful of dispersion curves could be picked for the virtual source gathers. Longer recordings of well-distributed impulsive sources or an overall more uniform noise distribution would improve the quality of the virtual sources.

P waves are best generated not by the background ambient noise but from subsurface sources such as earthquakes and active shots. The coda of these sources is providing most of the energy needed for body-wave interferometry. A similar result was observed by Lin an Tsai (2013), who showed that global body waves could be produced using the coda of large global earthquakes. Fortunately, our dataset contained over 300 natural and induced microearthquakes in addition to over 100 shots both on and off line, producing P-waves in the virtual source gathers at 20-35 Hz. The P-waves have the same apparent velocities as for nearby explosive shots. The virtual sources are much weaker than the explosive sources, but are much more densely spaced to enable higher-resolution near-surface imaging. The seismic reflection image created from the

virtual source gathers is of low quality, but is consistent with the highly faulted and hydrothermally altered stratigraphy of the geothermal field and surrounding valley.

REFERENCES

Aki, K. and Richards, P. G., 1980, *Quantitative Seismology: Theory and Practice,* W.H. Freeman, New York, p. 487-493, Print.

Barker, T. G. and Stevens, J. L., 1983, Shallow shear-wave velocity and Q-structures at the El-Centro strong motion accelerograph array, *Geophysical Research Letters*, **10**, No. 9, p. 853-856, doi: 10.1029/GL010i009p00853

Batzle, M. L. and Simmons, G., 1976, Microfractures in rocks from two geothermal areas, *Earth and Planetary Science Letters,* **30,** No. 1, 71-93

Bensen, G. D., Ritzwoller, M. H., Barmin, M. P., Levshin, A. L., Lin, F., Moschetti, M. P., Shapiro, N. M., and Yang, Y., 2007. Processing seismic ambient noise data to obtain reliable broad-band surface wave dispersion measurements, *Geophysical Journal International,* **169**, 39–1260. doi: 10.1111/j.1365-246X.2007.03374.x

Bianco, E., 2012, Volume-based seismic and rock physics analysis for geothermal reservoir characterization. *Presented at the 2012 SEG IQ Earth Forum*, **2012,** Avon, Colorado.

Boaga, J., Cassiani, G., Strobbia, C., and Vignoli, G., 2013. The role of Rayleigh waves ellipticity in mode misidentification. *Gruppo Nazionale di Geofisica Della Terra Solida,* **2013,** Trieste, Italy

Bonner, B, Hutching, L., and Kasameyer, P., 2006. A Strategy for Interpretation of Microearthquake Tomography Results in the Salton Sea Geothermal Field Based upon Rock Physics Interpretations of State 2-14 Borehole Logs, *Geothermal Resource Council Annual Meeting*, **2006**, San Diego, California

Brothers, D., Kilb, D., Luttrell, K., Driscoll, N., and Kent, G., 2011, Loading of the San Andreas fault by flood-induced rupture of faults beneath the Salton Sea. *Nature Geoscience.* **4,** 486-492, doi: 10.1038/NGEO1184

Browne, P. R. L., 1978, Hydrothermal alteration in active geothermal fields, *Annual review of earth and planetary sciences*. **6**. Annual Reviews, Inc., Palo Alto, Calif., p. 229-250.

Byerly, K., Brown, L., Voight, B., and Miller, V., 2010, Reflection imaging of deep structure beneath Montserrat using microearthquake sources, *Geophysical Research Letters* **Vol. 37**, L00E20, doi:10.1029/2009GL041995

Campillo, M. and Paul, A., 2003. Long-range correlations in the diffuse seismic coda, *Science*, **299**, 547–549.

Chan, M. A., and Tewhey, J. D., 1977. Subsurface structure of the southern portion of the Salton Sea Geothermal, *Lawrence Livermore Laboratory,* Rept UCRL-52267

Claerbout, J. F., 1968, Synthesis of a layered medium from its acoustic transmission response, *Geophysics*, **33**, 264–269

Daley, T.M., McEvilly, T.V. and Majer, E.L., 1988. Analysis of P and S Wave Vertical Seismic Profile Data from the Salton Sea Scientific Drilling Project." *Journal of Geophysial Research,* **93**, No. B11, 13,025–13,036

Dept. of Energy, 2004, Federal Geothermal Research Program Update for Fiscal year 2003, *Report DOE/NE-ID-11147*

Dibblee, T. W., 1954, Geology of the Imperial Valley region, California, *Bulletin of California Department of Mines,* **170,** 21-28

Dong, S., He, R., and Schuster, G., 2006, Interferometric prediction and least squares subtraction of surface waves, *SEG 76th Annual International Meeting*, Expanded Abstracts, 2783–2786.

Dorsey, R., 2010, Sedimentation and recycling along an active oblique-rift margin: Salton Trough and northern Gulf of California. *Geology.* **38,** No. 5, 443-446. Doi: 10.1130/G30698.1

Draganov, D., Wapenaar, K., Mulder, W., Singer, J., and Verdel, A., 2007, Retrieval of reflections from seismic background-noise measurements, *Geophysical Research Letters,* **34**, L04305, doi:10.1029/2006GL028735.

Draganov, D., Campman, X., Thorbecke, J., Verdel, A., and Wapenaar, K., 2009. Reflection images from ambient noise, *Geophysics*, **74**, A63–A67, doi:10.1190/1.3193529.

Dutcher, L. C., Hardt, W. F. and Moyle, Jr., W. R., 1972, Preliminary Appraisal of Ground Water in Storage with Reference to Geothermal Resources in the Imperial Valley Area, California, *U.S. Geological Survey*, Washington, D. C., Circular 649

Elders, E. A. and Sass, J. H., 1988, The Salton Sea Scientific Drilling Project, *Journal of Geophysical Research,* **93,** No. B11, 12953-12968

Elders, W.A., 1989, Geothermal resource assessment of the Salton Sea geothermal field, California: University of California, *Riverside*, Rept. UCR/IGPP/89-32, 4 p

Forghani, F., and Snieder, R., 2010, Underestimation of body waves and feasibility of surface-wave reconstruction by seismic interferometry, *Leading Edge*, **29**, 790–794, doi:10.1190/1.3462779

Fuis, G.S., and Kohler, W.H., 1984, Crustal structure and tectonics of the Imperial Valley region, California in The Imperial basin – Tectonics, sedimentation, and thermal aspects, *Soceity of Economic Paleontology and Minerology, Pacific Section,* 1-13.

Foti, S., 2000, Multistation Methods for Geotechnical Characterization using Surface Waves, *PHD Thesis,* Politecnico di Torino, doi:10.6092/polito/porto/2497212

Gritto, R. and Majer, E. L., 2003, Seismic Methods for Resource Exploration in Enhanced Geothermal Systems, *Geothermal Resources Council Transactions*, **27**, 223-226, LBNL-52967

Han, L., Hole, J. A., Delph, J. R.[1], Livers, A. J., White-Gaynor, A., Stock, J. M., Fuis, G., Driscoll, N. W., Kell, A. M., and Kent, G., 2013, Active rifting processes in the central Salton Trough, California, constrained by the Salton Seismic Imaging Project (SSIP), *Presented at the American Geophysical Meeting Annual Meeting,* **2013,** Oral.

Haney, M. H., Wijk, K. V., Preston, L. A. and Aldridge, D. F., 2009, Observation and Modeling of Source Effects in Coda Wave Interferometry at Pavlof Volcano. *The Leading Edge.* **28.** 554-560.

Helgeson, H. C., 1968, Geologic and thermodynamic characteristics of the Salton Sea geothermal system, *American Journal of Science,* **266,** 129-166.

Herzig, C.T., Mehegan, J.M., and Stelting, C.E., 1988, Lithostratigraphy of the State 2-14 borehole, Salton Sea scientific drilling project: *Journal of Geophysical Research*, **93,** 12,969-12,980.

Holland, A., 2002, Microearthquake Study of the Salton Sea Geothermal Field, California: Evidence of Stress Triggering, *M.S. Thesis,* University of Texas, El Paso, TX.

Hulen, J.B. and Pulka, F.S., 2001. Newly-discovered, ancient extrusive rhyolite in the Salton Sea geothermal field, Imperial Valley, California – Implications for reservoir characterization and duration of volcanism in the Salton trough: *Stanford University 26th Workshop on Geothermal Reservoir Engineering*, Proceedings, 10 p.

Hulen, J.B., Kaspereit, D., Norton, D.L., Osborn, W., and Pulka, F.S., 2002, Refined conceptual modeling and a new resource estimate for the Salton Sea geothermal field, Imperial Valley, California: *Geothermal Resources Council Transactions*, **26**, 29-36.

Hulen, J.B., Norton, D.L., Moore, J.N., Osborn, W., van de Putte, T., and Kaspereit, D., 2003, The role of sudden dilational fracturing in evolution and mineralization of the southwestern Salton Sea geothermal system, California, *Stanford University*, 28th Workshop on Geothermal Reservoir Engineering, 25 p.

Ivanov, J., Park, C. B., Miller, R. D., Xia, J., 2001, Modal Separation before Dispersion Curve Extraction by MASW Method, *Proceedings of the SAGEEP 2001*, Denver, Colorado, SSM-3

Janecke, S.U., Kirby, S.M., Langenheim, V.E., Steely, A.N., Dorsey, R.J., Housen, B., and Lutz, A.T., 2005, High geologic slip rates on the San Jacinto fault zone in the SW Salton Trough, and possible near-surface slip deficit in sedimentary basins, *Geological Society of America Special Paper*, **475**, 48 p., doi:10.1130/2010.2475

Kasameyer, P. W., Younker, L. W. and Hanson, J. M., 1984, Development and application of a hydrothermal model for the Salton Sea geothermal field, California, *Geological Society of America Bulletin,* **95**, 1242-1252.

Kirby, S. M., Janecke, S. U., Dorsey, R. A., Housen, B. A., Langenheim, V. E., McDougall, K. A. and Steely, A. N., 2007, Pleistocene Brawley and Ocotillo Formations: Evidence for Initial Strike-Slip Deformation along the San Felipe and San Jacinto Fault Zones, Southern California*, The Journal of Geology*, **115**, p. 43–62

Lin, F. C., Moschetti, M. P. and Ritzwoller, M. H., 2008, Surface wave tomography of the western United States from ambient seismic noise: Rayleigh and Love wave phase velocity maps, *Geophysical Journal International,* **173,** No.1, 281-298, doi:10.1111/j.1365-246X.2008.03720.x

Lin, F., Dunzhu, L., Clayton, R. W., and Hollis, D., 2013, High-resolution 3D shallow crustal structure in Long Beach, California: Application of ambient noise tomography on a dense seismic array, *Geophysics,* **78,** No. 4, Q45-Q56. doi:10.1190/GEO2012-0453.1

Lin, F.C., V. C. Tsai, B. Schmandt, Z. Duputel, and Z. Zhan, 2013, Extracting seismic core phases with array interferometry, *Geophysical Research Letters,* **40**, 1049-1053, doi:10.1002/grl.50237

Livers, A. J., Han, L., Delph, J., White-Gaynor, A., Petit, R., Hole, J. A., Stock, J. M. and Fuis, G. S., 2012. Tomographic characteristics of the northern geothermally active rift zone of the Imperial Valley and its rift margins: Salton Seismic Imaging Project (SSIP). *American Geophysical Union Annual Meeting,* **2012,** San Francisco, CA.

Lonsdale, P.F., 1989. Geology and tectonic history of the Gulf of California, In: Winterer, E.L., Hussong, D.M., Decker, R.W. (Eds.), The Eastern Pacific Ocean and Hawaii. Geological Society of America, Boulder, pp. 499–521

Louie, J. N., 2001, Faster, better: Shear-wave velocity to 100 meters depth from microtremor arrays, *Bulletin of the Seismological Society of America*, **91,** No. 2, 347-364

Lutz, A. T., Dorset, R. J., Housen, B. A. and Janecke, S. U., 2006, Stratigraphic record of Pleistocene faulting and basin evolution in the Borrego Badlands, San Jacinto fault zone, Southern California, *Geological Society of America Bulletin*, **118**, no. 11/12, p. 1377–1397, doi:10.1130/B25946.1

Lynch, D. K. and Hudnut, K. W., 2008. The Wister Mud Pot Lineament: Southeastward Extension or an Abandoned Strand of the San Andreas Fault?, *Bulletin of the Seismological Society of America,* **98,** No. 4, 1720-1729, doi:10.1785/0120070252

McDowell, S. D., Elders, W. A., 1983. Allogenic layer silicate minerals in borehole Elmore # 1, Salton Sea Geothermal Field, California, *American Minerology,* **68,** 1146-1159,

McKibben, M.A., and Andes, J. P., 1986. Ore Mineralization and Related Fluid Inclusion Properties in the SSSDP Cores. *Geothermal Resources Council Meeting*, Palm Springs, CA.

McMechan, G.A., and Yedlin, M.J., 1981, Analysis of dispersive waves by wave field transformation, *Geophysics*, **46**, 869-874.

Meidav, T. and Fergerson, R., 1972, Resistivity studies of the Imperial Valley geothermal area, California, *Geothermics,* **1**, 47-62.

Morse, J. G., 1977. Well Interference Study of the Multi-Layered Salton Sea Geothermal Reservoir. *Lawrence Livermore Laboratory.*

Muramoto, F. S., Elders, W. A., 1984. Correlation of Wireline Log Characteristics' with Hydrothermal Alteration and Other Reservoir Properties of the Salton Sea and Westmorland Geothermal Fields, Imperial Valley, California, USA, *Los Alamos National Laboratory.*

Norton, D. L., and Hulen, J. B., 2006, Magma-Hydrothermal Activity in the Salton Sea Geothermal Field, Imperial County, California, *GRC Transactions,* **30,** 991-998

O'Neill, A. and Matsuoka, T., 2005, Dominant Higher Surface-wave Modes and Possible Inversion Pitfalls, *Journal of Environmental and Engineering Geophysics*, **10**, No. 2, 185–201

Paillet et al., 1986, Preliminary report on Geophysical Well-logging Activity on the Salton Sea Scientific Drilling Project, Imperial Valley, California, *U. S. Geological Survey Open File Report*, 86-544

Park, C.B., Miller, R.D., and Xia, J., Hunter, J.A., and Harris, J. B., 1999a, Higher mode observation by the MASW method, *SEG Annual Meeting,* **1999***,* Houston, TX

Park, C.B., Miller, R.D., and Xia, J., 1999b, Multi-channel analysis of surface waves (MASW), *Geophysics,* **64**, 800 – 808.

Park, C.B., Miller, R.D., and Xia, J., 1999c, Multimodal analysis of high frequency surface wave, *Symposium on the Application of Geophysics to Engineering and Environmental Problems*, **99,** p. 115-122.

Rogers. D. A., 1980, Analysis of pull-apart basin development produced by *en echelon* strike-slip faults. *Special Publication International Association of Sedimentology,* **4,** 27-41

Roux, P., Sabra, K. P., Gerstof, P., and Kuperman, W. A., 2005, P-wavesfrom cross-correlation of seismic noise, *Geophysical Research Letters,* **32**, L19303, doi:10.1029/2005GL023803

Ryberg, T., 2011, Body wave observations from cross-correlations of ambient seismic noise: A case study from the Karoo, RSA. *Geophysical Research Letters*, **38**, L13311, doi:10.1029/2011GL047665

Saygin, E. and Kennett, B. L. N., 2012, Crustal structure of Australia from ambient seismic noise tomography, *Journal of Geophysical Research: Soild Earth,* **117,** No. B01304, doi:10.1029/2011JB008403

Sabra, K.G., Gerstoft, P., Roux, P., Kuperman,W.A. & Fehler, M.C., 2005, Extracting time-domain Green's function estimates from ambient seismic noise, *Geophysical Research Letters,* **32**, L03310, doi:10.1029/2004GL021862.

Schmitt, A. K. and Hulen, J. B., 2008, Buried rhyolites within the active, high-temperature Salton Sea geothermal system, *Journal of Volcanology and Geothermal Research,* **178,** 708-718. doi:10.1016/j.jvolgeores.2008.09.001

Schuster, G. T., 2010, *Seismic Interferometry,* Cambridge: Cambridge UP. Print.

Scroeder, R. C., 1976, Reservoir Engineering Report for the Magma-SDG&E Geothermal Experiment Site near the Salton Sea Geothermal Filed, California. *Lawrence Berkeley Laboratory*

Setyowiyoto, J., 2012, Characterization, pressure, and temperature influence on elastic wave velocities in carbonate rocks and their relationships, *PHD Thesis,* Universiti Teknologi, Malaysia.

Shapiro, N. M., Campillo, M., Stehly, L., and Ritzwoller, M. H., 2005. High-resolution surface wave tomography from ambient seismic noise, *Science*, **307**, 1615–1618.

Sneider, R., 2004, Extracting the Green's function from the correlation of coda waves: A derivation based on stationary phase. *Phys. Rev. E*. **69,** No. 4

Stokoe II, K.H., Wright, G.W., Bay, J.A., and Roesset, J.M., 1994. Characterization of geotechnical sites by SASW method, in Geophysical characterization of sites, *ISSMFE Technical Committee #10*, New Delhi

Sturz, A., 1989, Low-temperature Hydrothermal Alteration in Near-surface Sediments, Salton Sea Geothermal Area, *Journal of Geophysical Research,* **94,** No. B4, 4015-4024

Svenson**,** H., Karlsen, D.A., Sturz, A, Backer-Owe, K., Banks, D.A., and Planke, S., 2007, Processes controlling water and hydrocarbon composition in seeps from the Salton Sea Geothermal System, California, USA, *Geology,* **35**, 85-88.

Sylvester, A. G. and Smith, R. R., 1976, Tectonic Transpression and Basement-Controlled Deformation in San Andreas Fault Zone, Salton Trough, California, *AAPG Bulletin,* **60,** No. 12. 225-261.

Tewhey, J. D., 1977, Geologic Characteristics of a Portion of the Salton Sea Geothermal Field, *Lawrence Livermore Laboratory,*

Towse, D. F. and Palmer, T. D., 1975, Summary of geology at the ERDA-Magma-SDG&E geothermal test site, UCID-17008, *Lawrence Livermore National Laboratory*, Livermore, California,

Tratt, D. M. and Hall, J.L., 2009, Remote Sensing of Geothermal Activity and Gaseous Emissions Along the Calipatria Fault in the Salton Sea Geothermal, Imperial County, California, *Southern California Earthquake Center Symposium,* **2009,** Poster.

Van de Kamp, P.C., 1973, Holocene continental sedimentation in the Salton basin, California: A reconnaissance, *Geological Society of America Bulletin,* **84**, 827-848,

Wapenaar, K., Thorbecke, J. W., and Draganov, D., 2002, Relations between reflection and transmission responses of a 3-D inhomogenous media, *Geophysical Journal International,* **156,** No. 2, 179-194

Wapenaar, K., 2002, Synthesis of an inhomogeneous medium from its acoustic transmission response, *Geophysics*, **68**, 1756–1759.

Wegler, U., Sens-Schonfelder, C., and Pryzbilla, J., 2007, Fault zone monitoring with passive image interferometry, *Geophysical Journal International,* **168.** No. 3, 1029-1033, doi:10.1111/j.1365-246X.2006.03284.x

Xia, J., Miller, R. D. and Park, C. B., 2002, Advantages of calculating shear-wave velocity from surface waves with higher-order modes. *SEG Technical Programs Expanded Abstracts.* **19,** 1295-1298

Xia, J., Miller, R. D., Park, C. B., and Tian, G., 2003, Inversion of high frequency surface waves with fundamental and higher modes, *Journal of Applied Geophysics,* **52,** 45–57

Younker, L. and Kasameyer, P. W., 1978, A revised estimate of recoverable thermal energy in the Salton Sea Geothermal resource area, UCRL-52450. *Lawrence Livermore National Laboratory*,

Younker, L. W., Kasameyer, P. W. and Tewhey, J. D., 1981, Geological, Geophysical, and Thermal Characteristics of the Salton Sea Geothermal Field, California, *Journal of Volcanology and Geothermal Research* **12,** 221-258,

APPENDIX A: LIST OF FIGURES

FIGURE 1 *TECTONIC MAP OF SOUTHWESTERN UNITED STATES AND NORTHWESTERN MEXICO.*

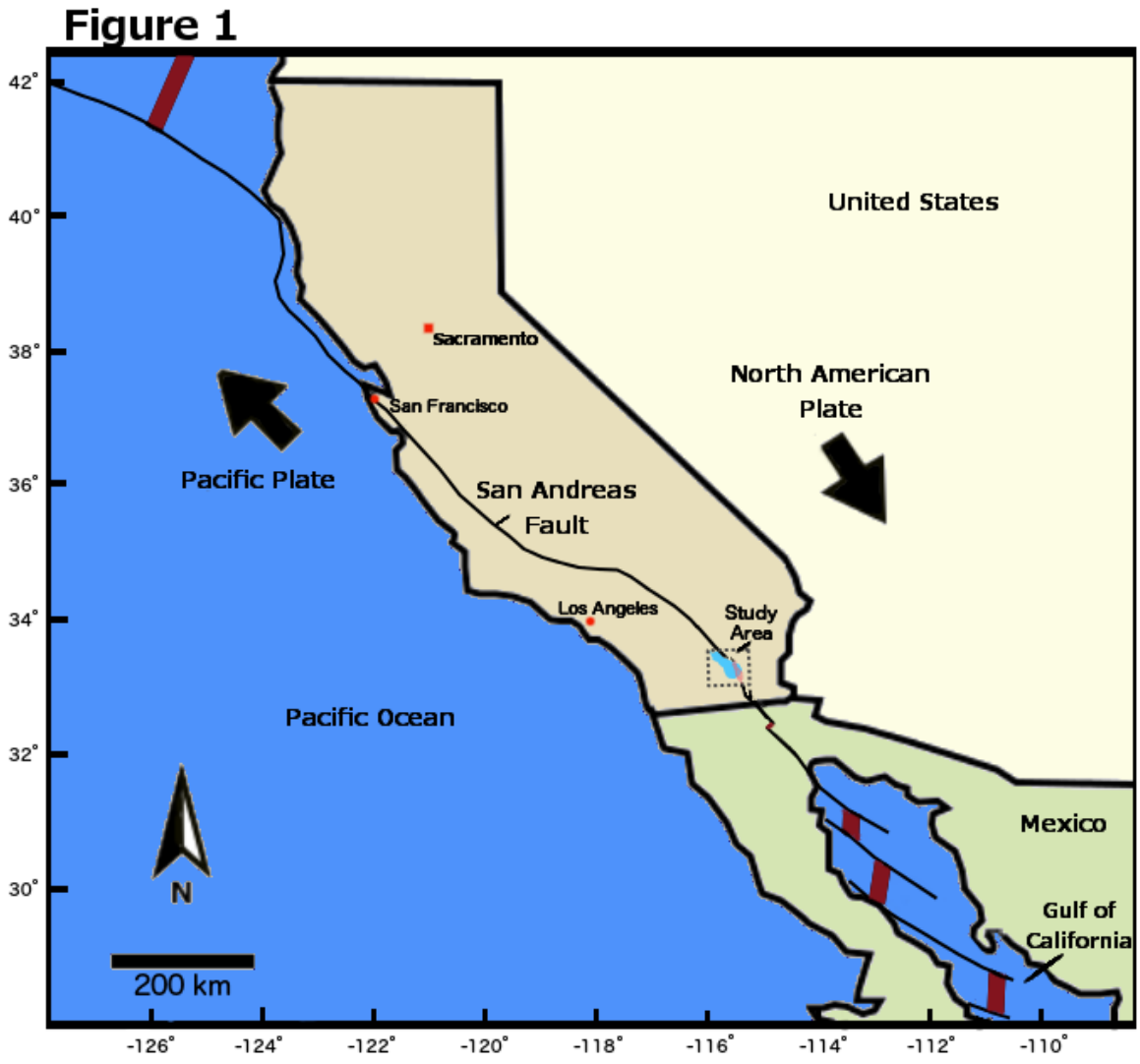

FIGURE 2 *MAP OF THE SALTON SEA STUDY AREA*

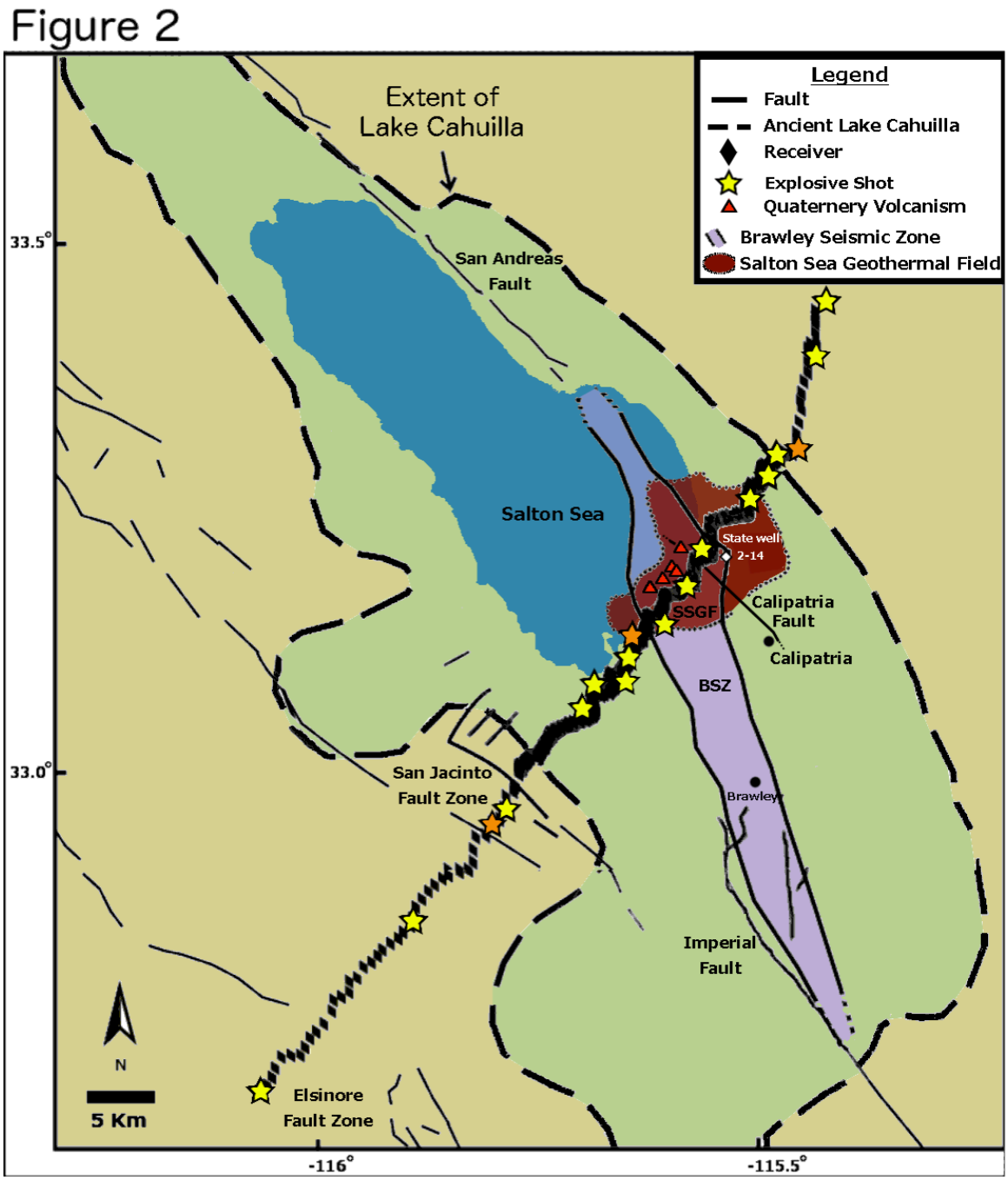

FIGURE 3 *STRATIGRAPHY FOR THE SALTON TROUGH AND SALTON SEA GEOTHERMAL FIELD WITH VELOCITY AND TEMPERATURE LOGS*

Figure 3

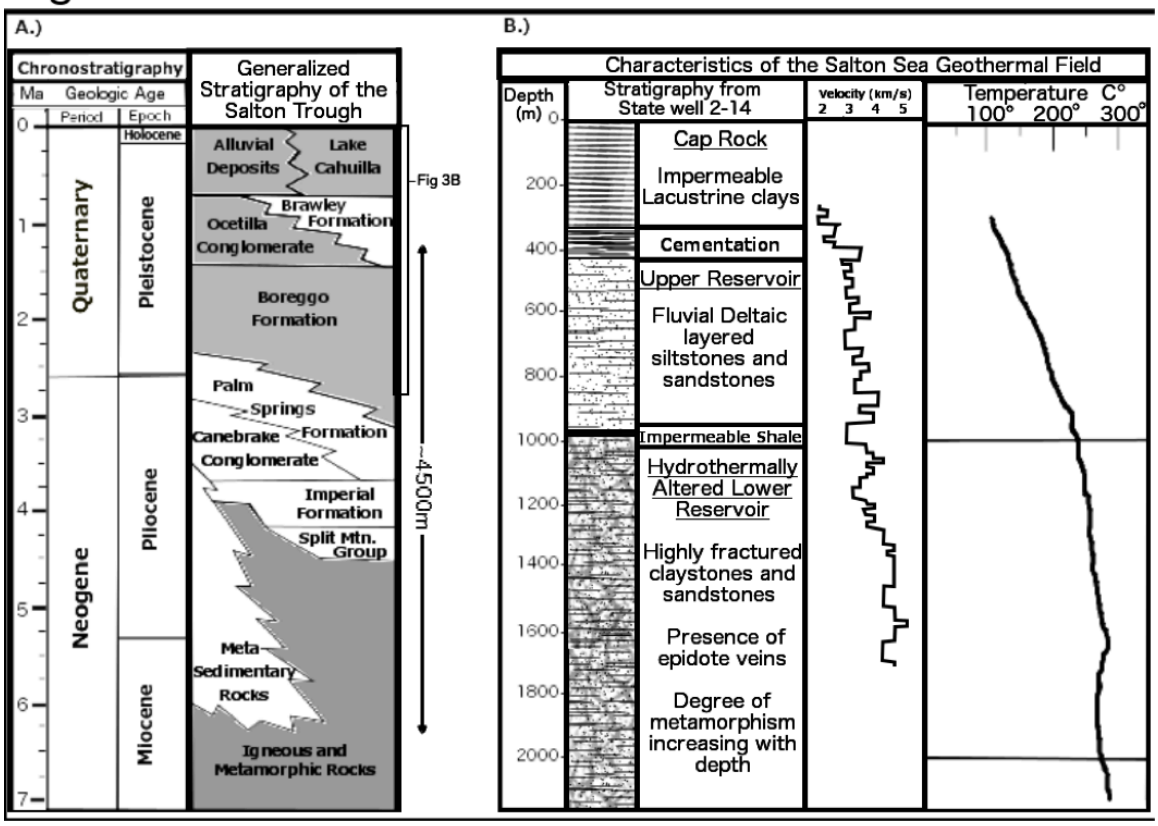

FIGURE 4 *RAW NOISE SECTION ACROSS SEISMIC LINE*

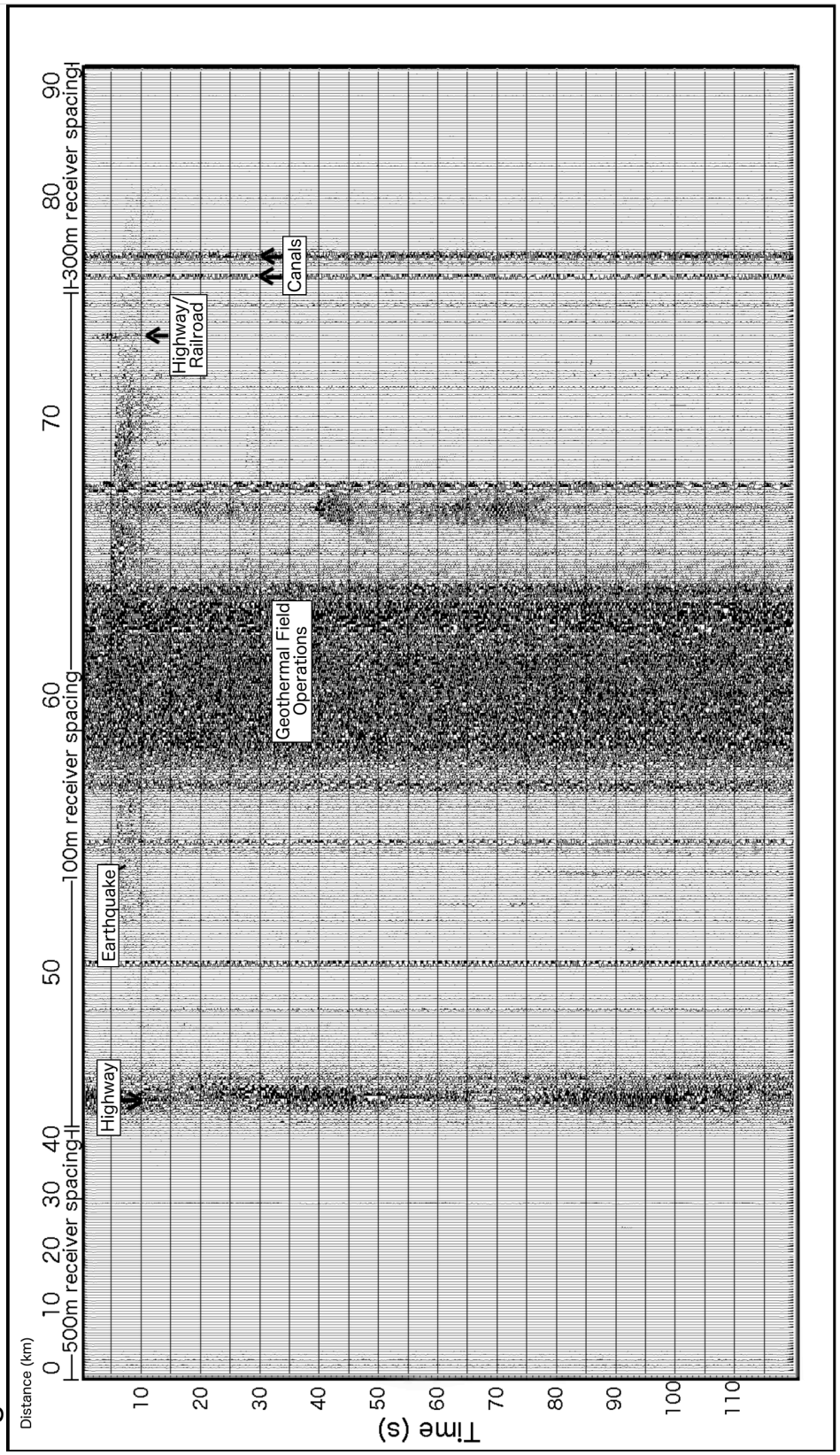

Figure 4

FIGURE 5 VIRTUAL SOURCE GATHER

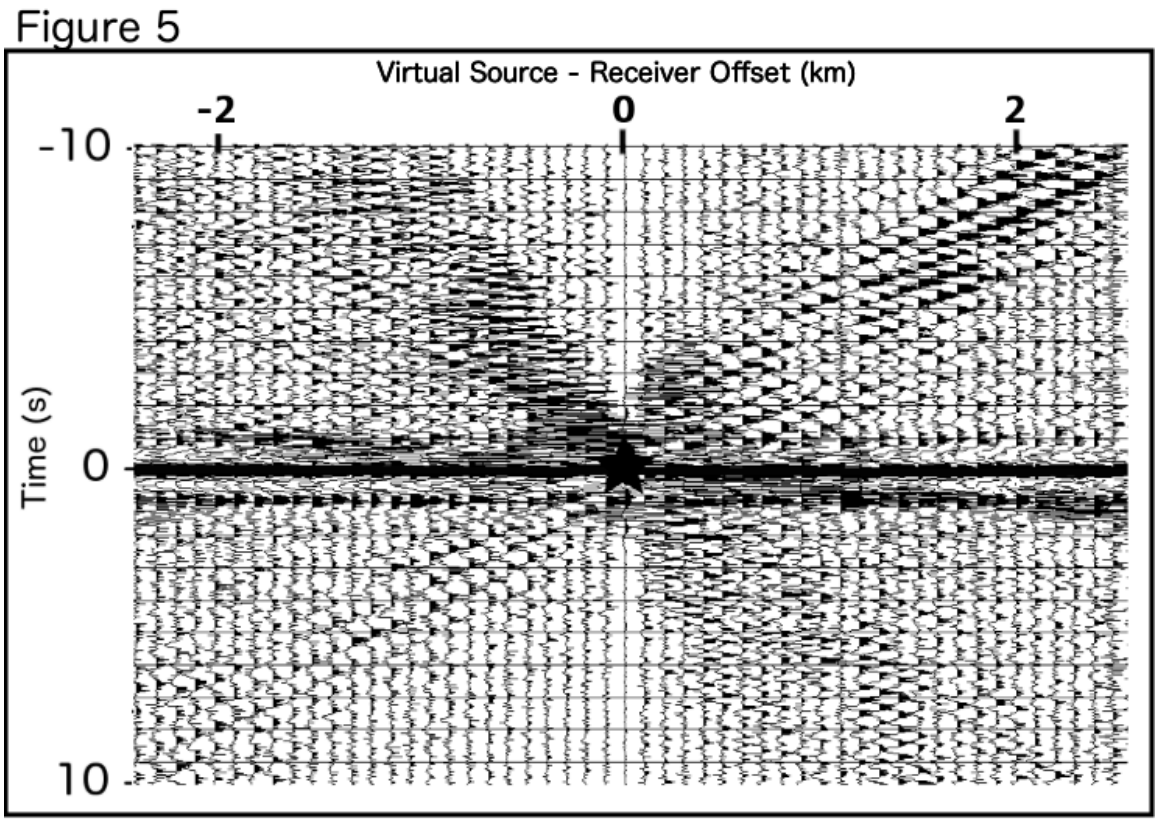

FIGURE 6 IMPULSIVE SOURCE ARTIFACT AND ARTIFACT REMOVAL

Figure 6

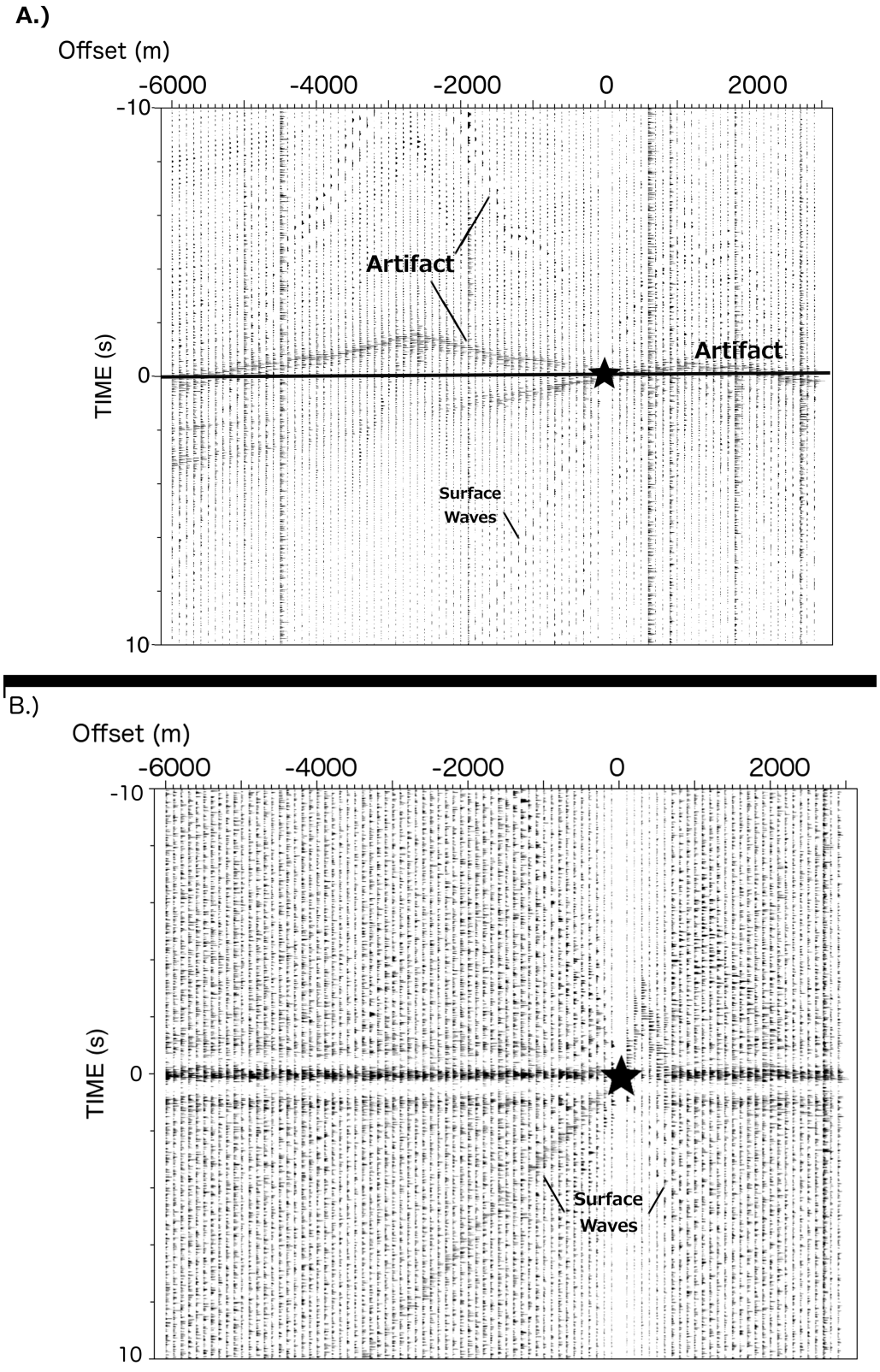

FIGURE 7 CONTINUOUS SOURCE ARTIFACTS

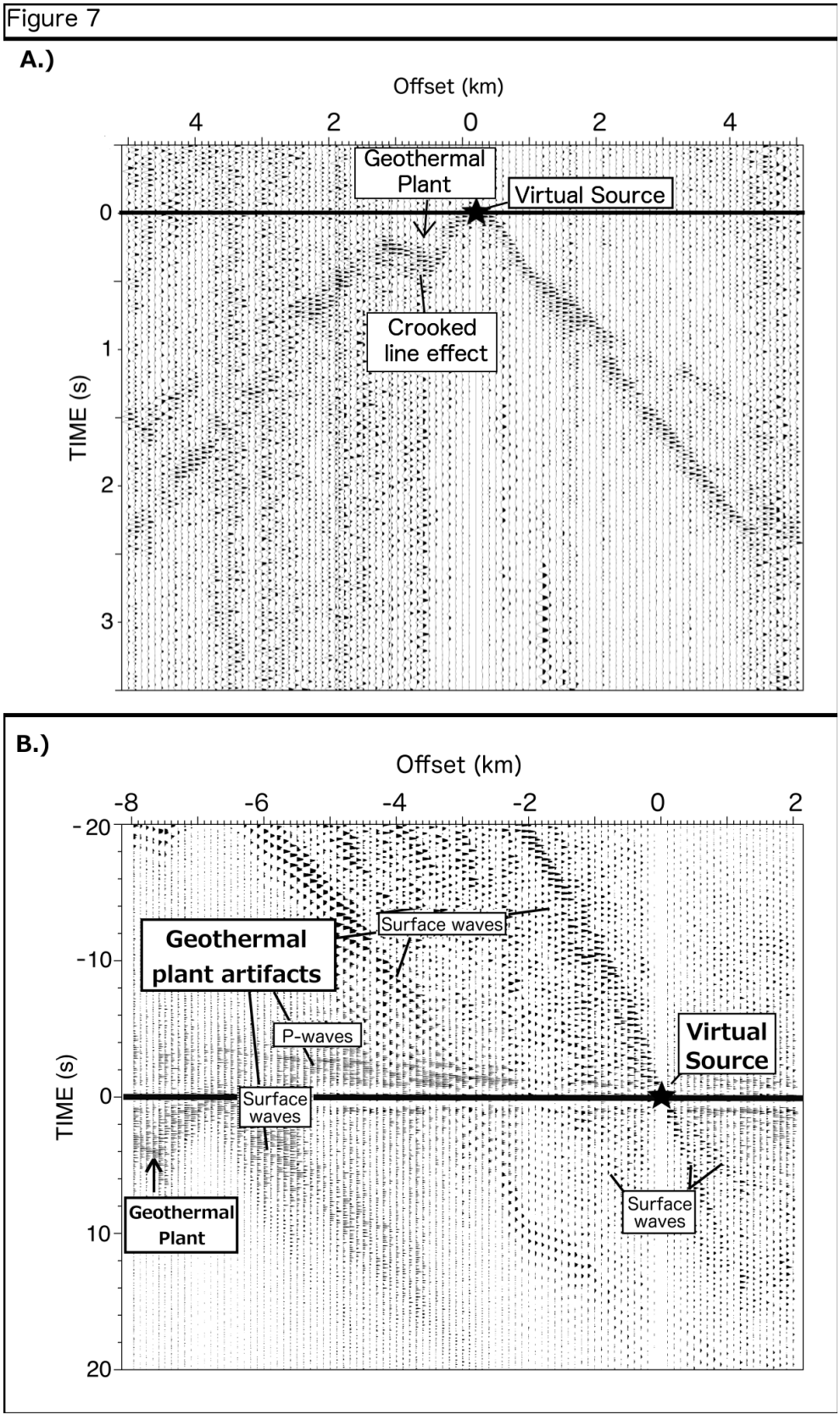

FIGURE 8 *CONTINUOUS SOURCE ARTIFACT AND REMOVAL*

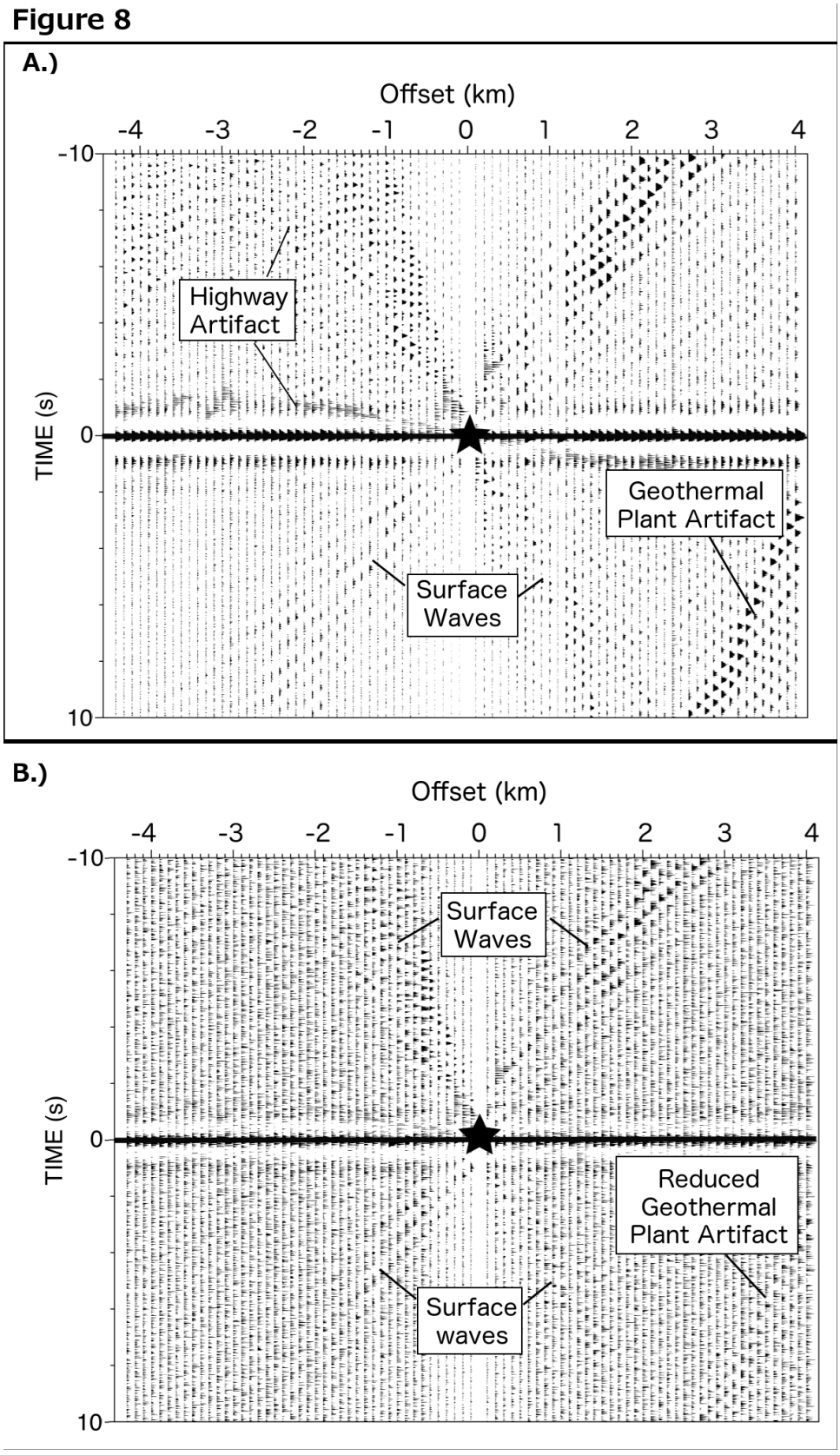

FIGURE 9 *MULTIMODAL SURFACE WAVES ON EXPLOSIVE SHOT AND VIRTUAL SOURCE GATHERS*

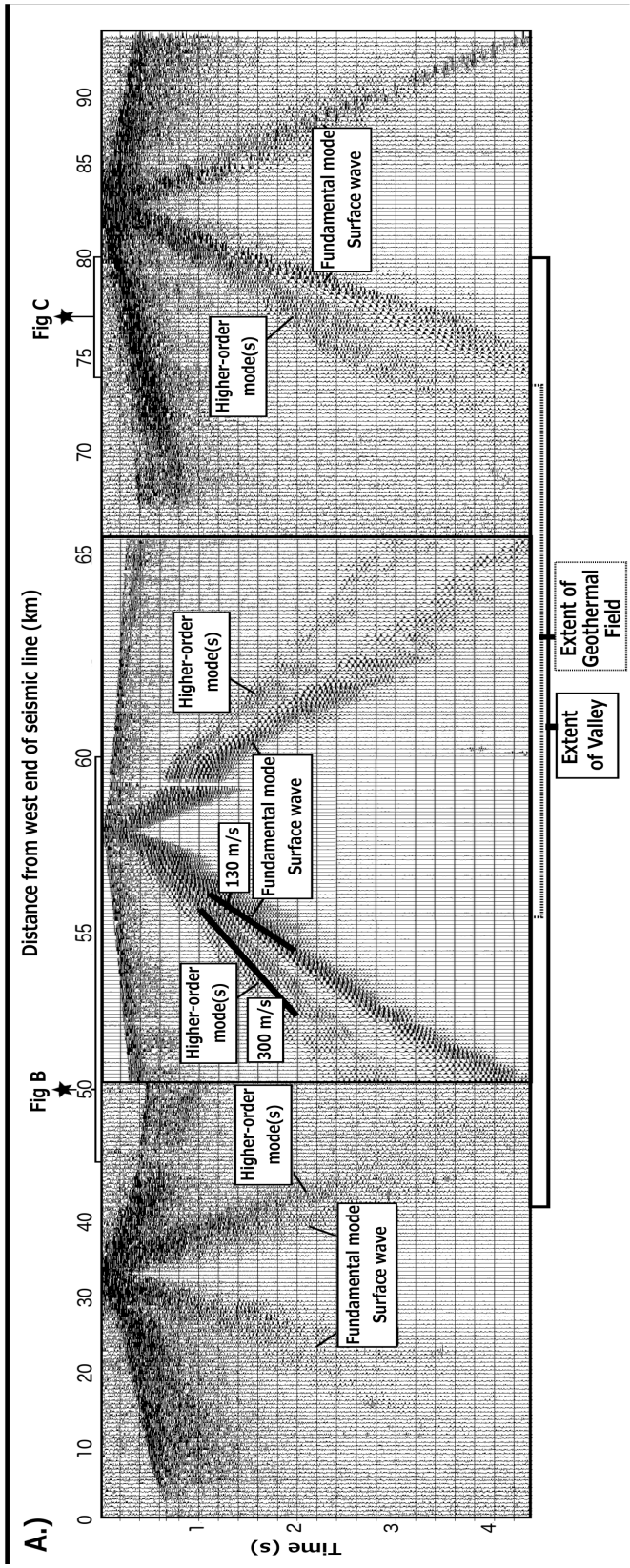

B.)

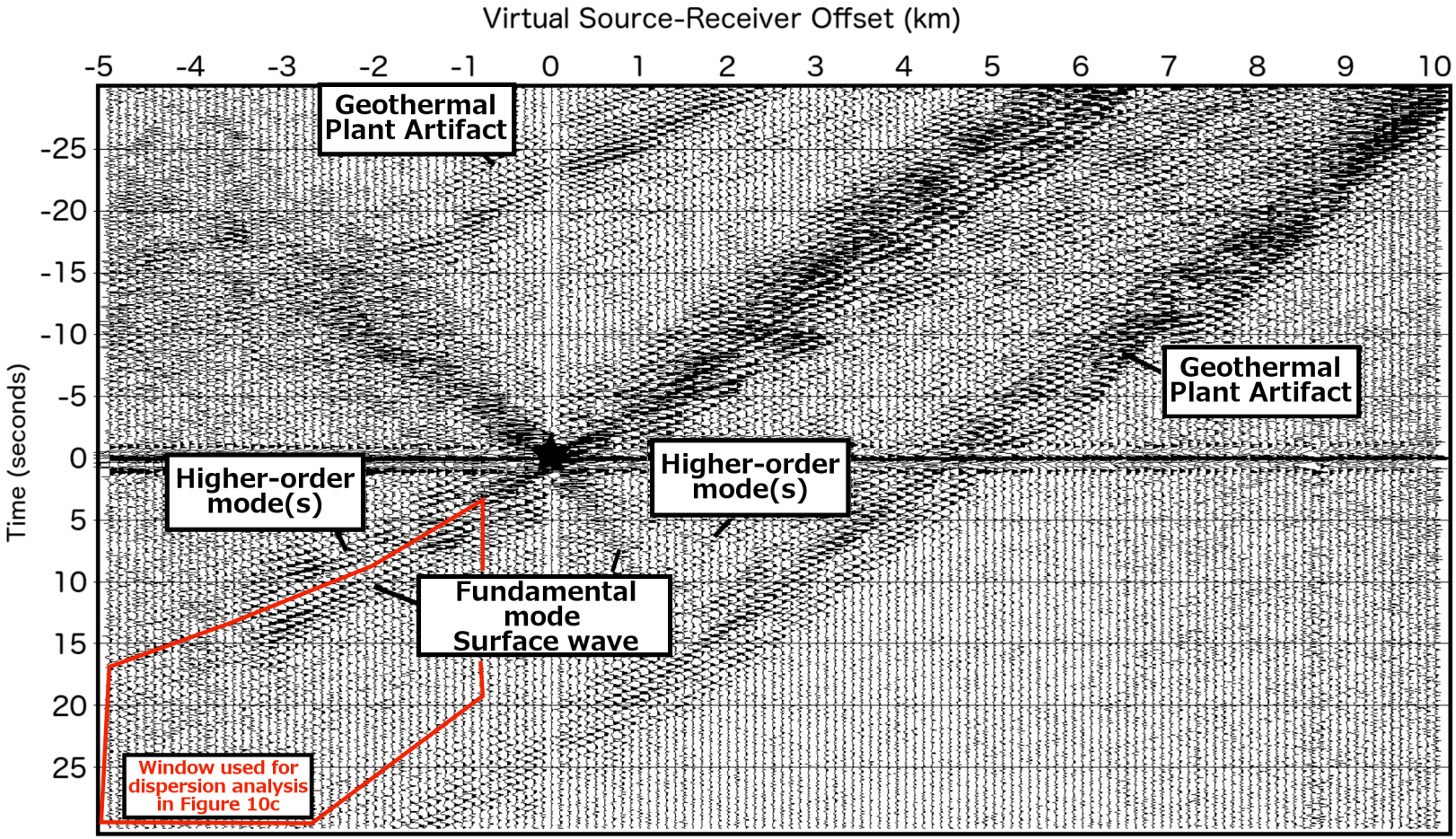
Virtual Source-Receiver Offset (km)
-5
-4
-3
-2
-1
0
1
2
3
4
5
6
7
8
9
10
Time (seconds)
-25
-20
-15
-10
-5
0
5
10
15
20
25
Geothermal Plant Artifact
Geothermal Plant Artifact
Higher-order mode(s)
Higher-order mode(s)
Fundamental mode Surface wave
Window used for dispersion analysis in Figure 10c

C.)

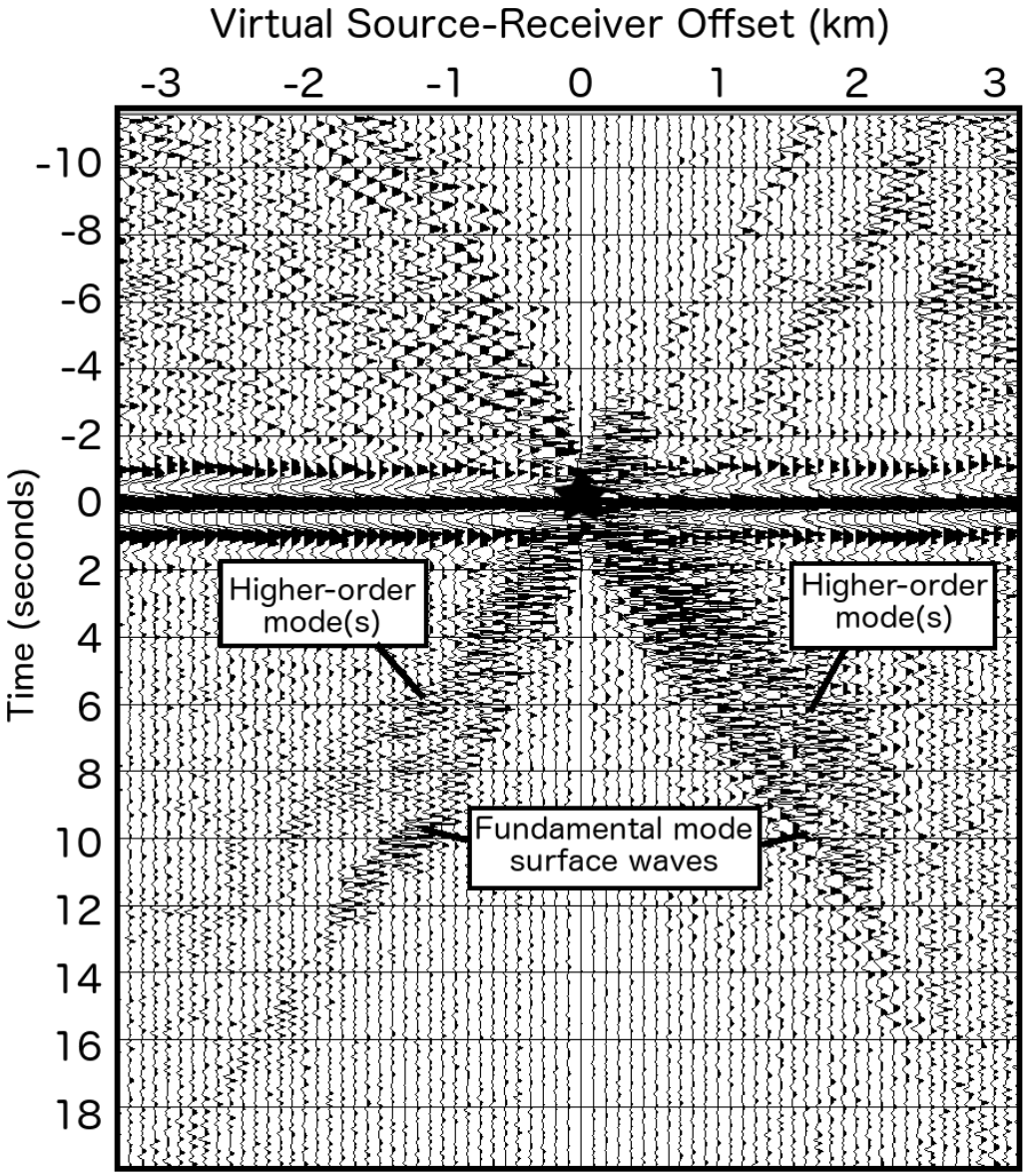
Virtual Source-Receiver Offset (km)
-3
-2
-1
0
1
2
3
Time (seconds)
-10
-8
-6
-4
-2
0
2
4
6
8
10
12
14
16
18
Higher-order mode(s)
Higher-order mode(s)
Fundamental mode surface waves

FIGURE 10 VIRTUAL SOURCE VS EXPLOSIVE SHOT SURFACE WAVE DISPERSION ANALYSIS

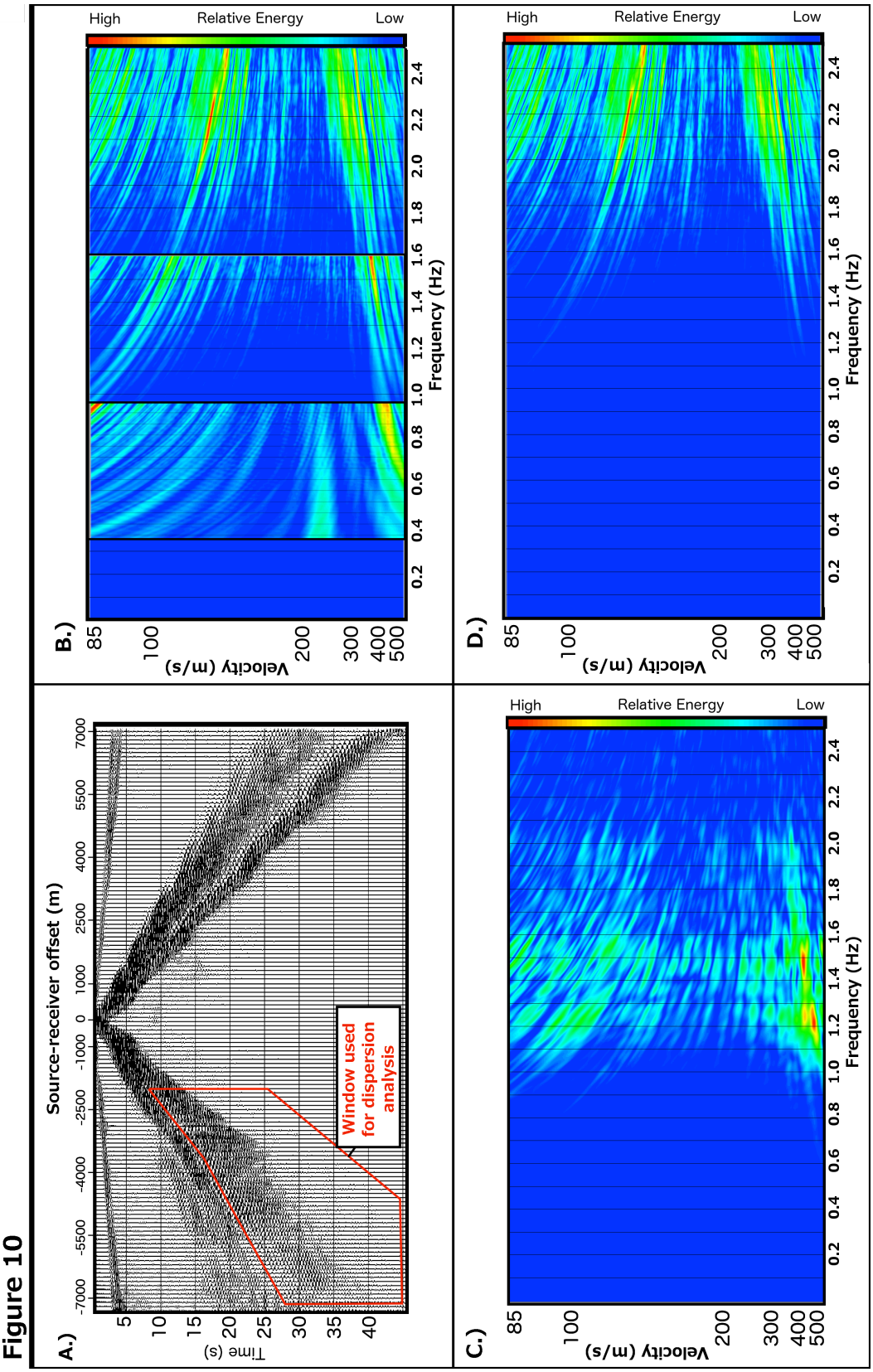

FIGURE 11 *DIRECT, REFRACTED, AND REFLECTED P-WAVES ON VIRTUAL SOURCE GATHER WITH COMPARISON TO NEARBY EXPLOSIVE SHOT GATHER*

Figure 11

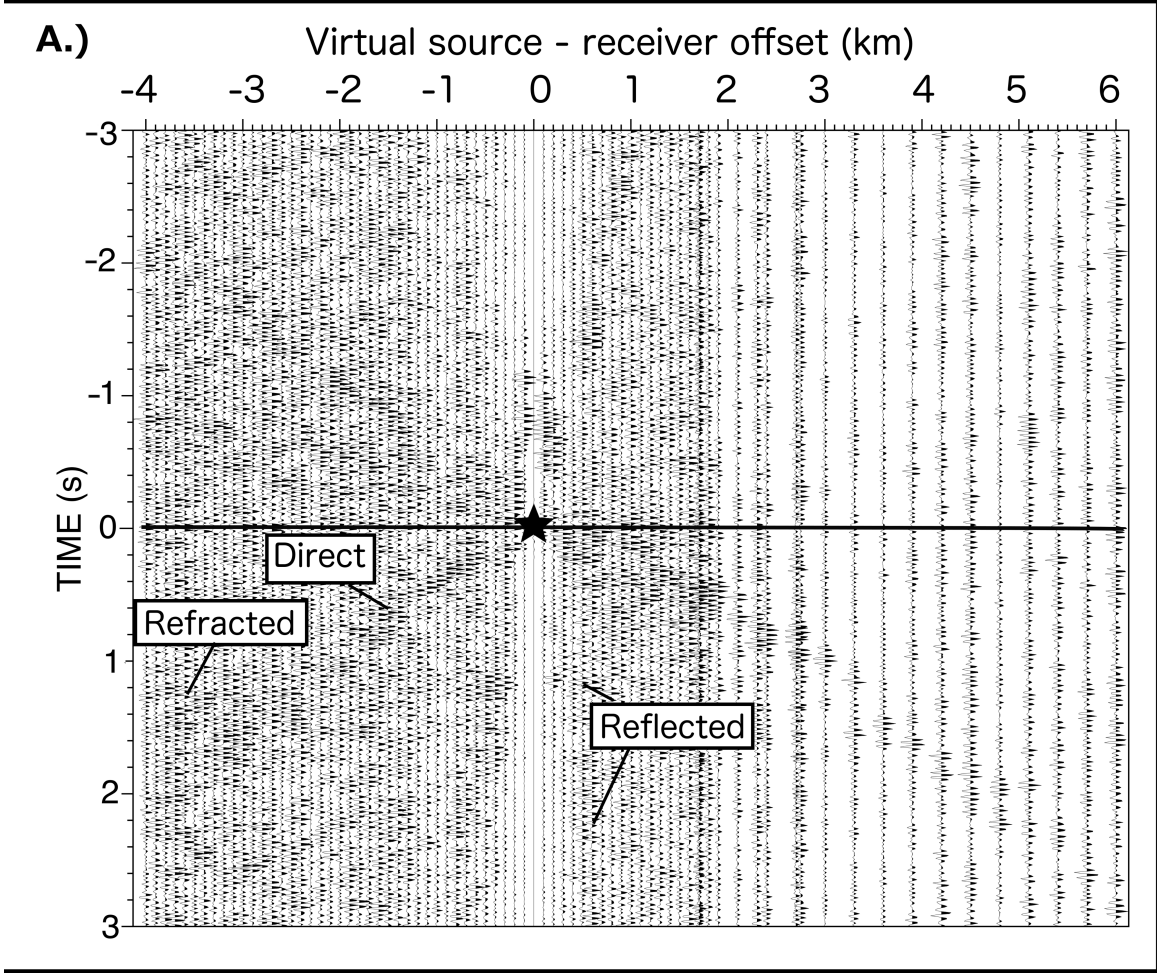

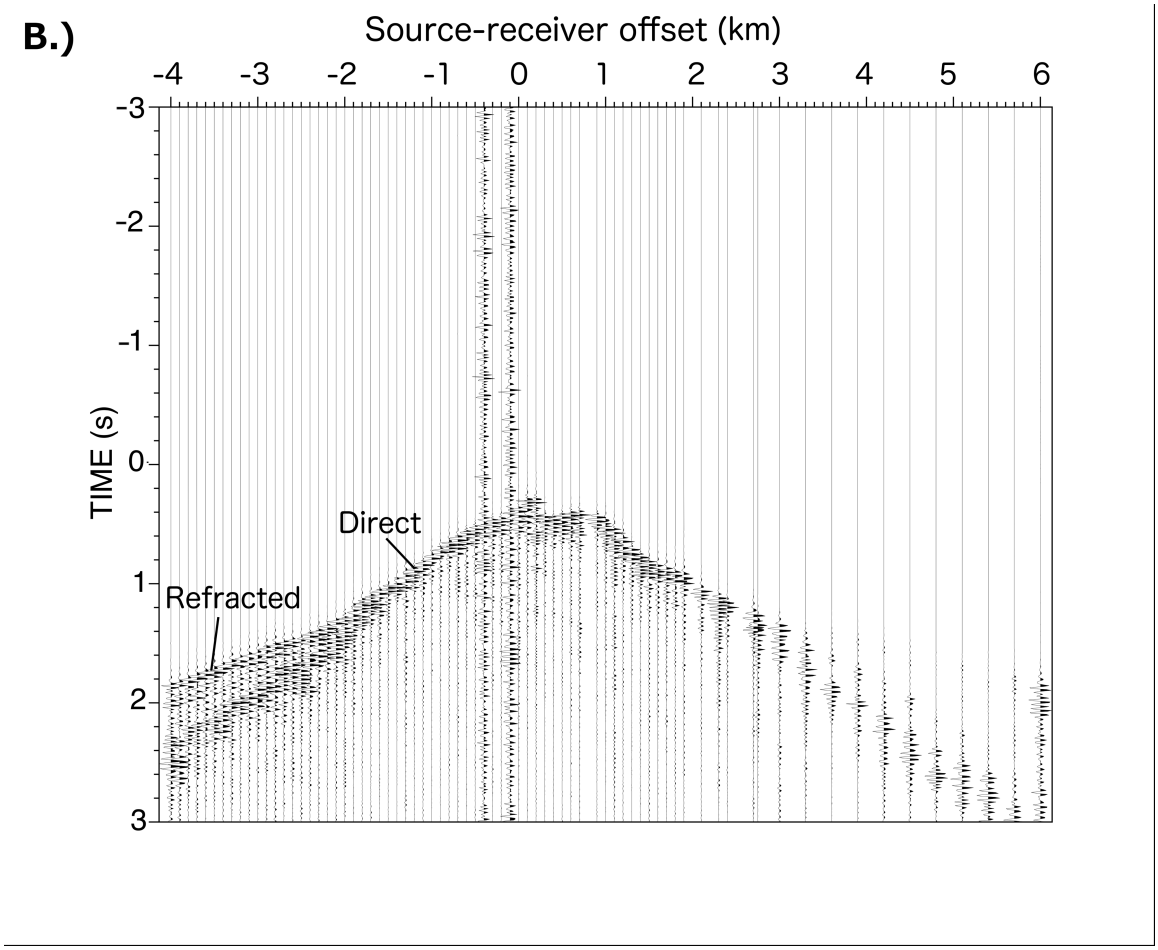
B.)
Source-receiver offset (km)
-4
-3
-2
-1
0
1
2
3
4
5
6
TIME (s)
-3
-2
-1
0
1
2
3
Direct
Refracted

FIGURE 12 *SEISMIC REFLECTION SECTION GENERATED FROM VIRTUAL SOURCE GATHERS*

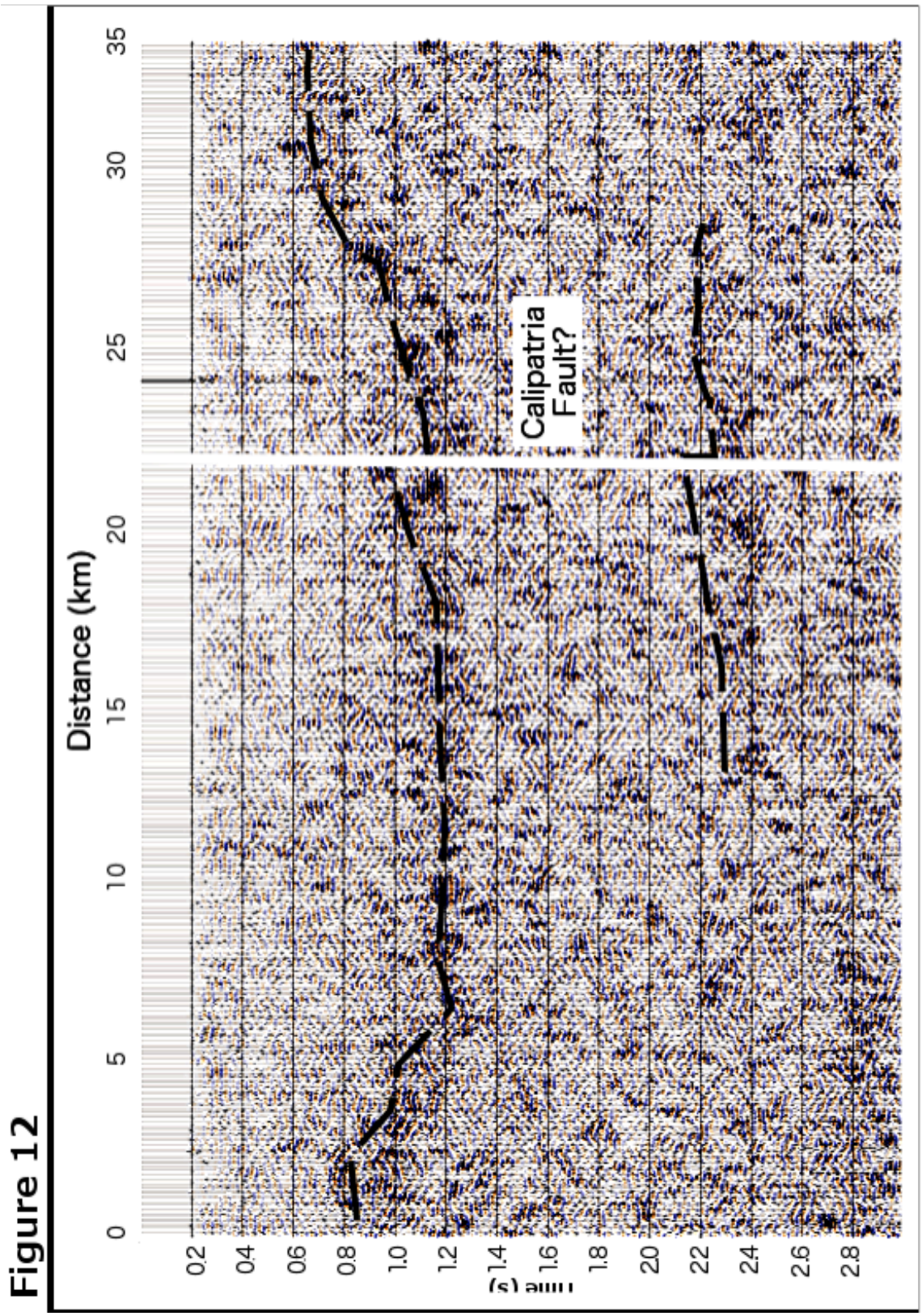

TABLES

TABLE 1 *PROCESSING FLOW FOR CREATION OF VIRTUAL SOURCE GATHERS.*

Virtual Source Gather Processing Flow	
Anti-alias Filter	*0.1-0.2-35-50
Resample	*8ms
Spectral Whitening	*0.1-0.2-35-50 Hz
Amplitude Normalization	*Automatic Gain Control 3s window
Cross-correlation	*Pilot receiver with all other receivers
Stacking	*All 2-minute windows

TABLE 2 *PROCESSING FLOW FOR CREATION OF DISPERSION CURVES*

Creation of Dispersion Curves	
Input raw data	*5km distance where modes are separated
Top Mute	*Remove body waves and higher order modes
Bandpass	*0.1-3Hz to remove body wave contamination
Tau-p Transform	*For fundamental mode velocities (85-100m/s)
Fourier Transform	*Transforms data into frequency-slowness

TABLE 3 PROCESSING FLOW FOR CREATION OF SEISMIC REFLECTION SECTION

Reflection Section Processing Flow

Preprocessing:

- **Assign geometry, creation of CMPs and binning**
- **Creation of Supergathers**
- **Mute direct waves**

Processing:

- **Spectral Shaping** *brighten frequencies P-waves are present
- **Bandpass Filter** *20-30Hz
- **Spherical Divergence Correction**
- **Normal Moveout Correction**
- **Bandpass Filter** *20-30Hz
- **CDP Stack**
- **Trace Mixing** *Laterally averages signal to boost reflectors